Co-condensation of proteins with single- and double-stranded DNA

Supplementary information

Supplementary figures

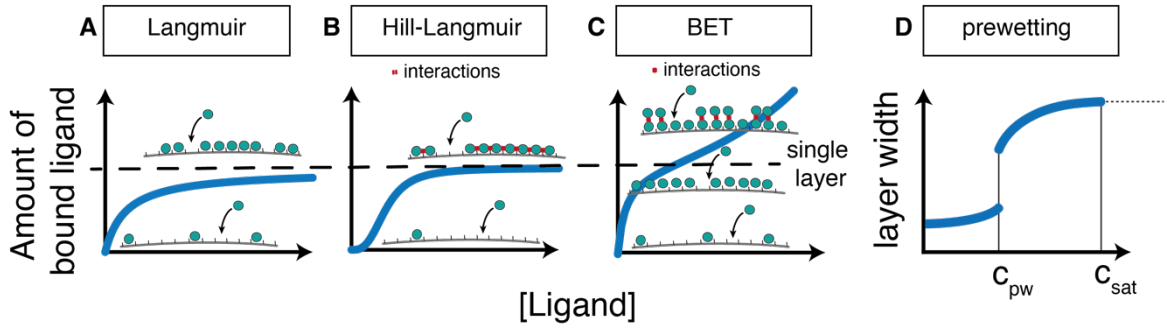

Figure S1. Ligand adsorption on substrates

The type of adsorption of ligands on a substrate depends in the relative strengths of ligand-ligand and ligand-substrate interactions.
(A) If ligand-ligand interactions are negligible, the ligands form a single layer on the substrate, with a lattice site occupancy that increases with increasing ligand concentration and approaches saturation at high ligand concentrations (Langmuir model).
(B) In presence of cooperative ligand-ligand interactions that support association with the substrate, the ligand occupancy of the scaffold follows a switch-like, sigmoidal trend. Increase of ligand concentration results in the formation of a single ligand layer on the scaffold (Hill-Langmuir model).
(C) In presence of attractive ligand-ligand interactions, association of ligands to a substrate can be described using the BET model. Increase in ligand concentration first leads to the formation of a single protein layer on the substrate and later to the formation of multiple layers of ligands on top of the initial layer. In contrast to the Langmuir and Hill-Langmuir model, ligand binding to the scaffold is non-saturable under this condition.
(D) The prewetting model is a continuum-description of adsorption of ligands with ligand-ligand interactions on a substrate. Below the so-called prewetting concentration of ligands, ligands form a thin layer in the substrate. Above the prewetting concentration, a thick layer of ligands on the substrate is formed. Above the saturation concentration for bulk phase separation of ligands, the layer thickness does not increase anymore.

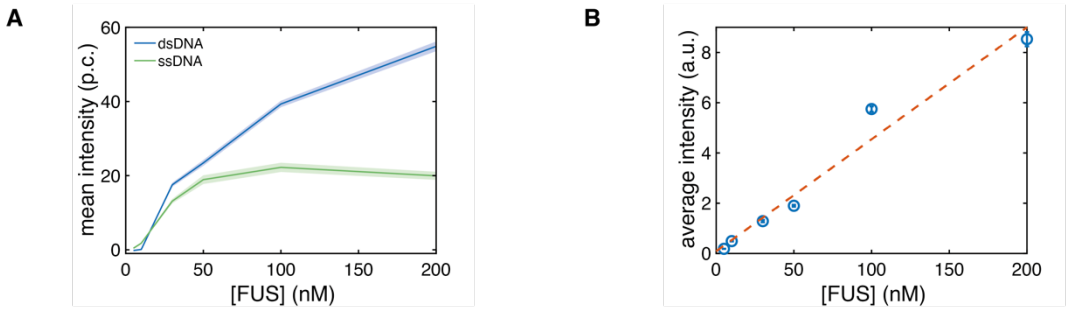

Figure S2. FUS adsorption on stretched DNA is saturable

(A) Equilibrium intensity of FUS on stretched dsDNA (blue) and stretched ssDNA (green) obtained from binding experiments performed with overstretched DNA at FUS concentrations between 5 and 200 nM (p.c.: photon count; mean ± SEM). Consistent with previous reports, FUS has higher affinity for ss than for dsDNA (1). (B) Background intensity as a function of protein concentration. To estimate FUS-dsDNA co-condensates concentration, images of FUS-dsDNA condensates in fully relaxed configuration (37 frames per DNA molecule) were first background subtracted and the maximum

intensity value was found for each image (average intensity of 200 ± 93 photon counts, mean over the time frames ± STD). The FUS-dsDNA co-condensates concentration was extrapolated from the calibration curve shown (slope = 0.045 [1/nM], intercept = 0.0908) to render an average concentration of 4.5 μM (N=15 condensates from DNA molecules with only 1 condensate each).

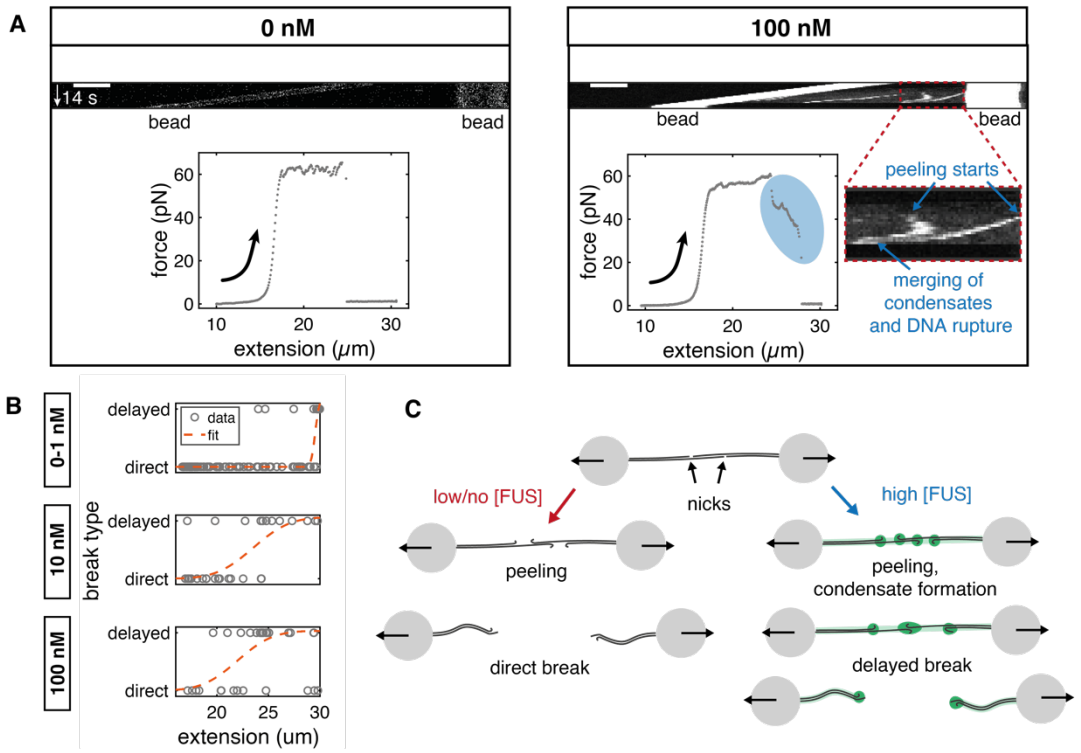

Figure S3. FUS adsorption delays DNA rupturing

(A) Kymographs and force-extension curves from DNA rupture experiments at 0 and 100 nM FUS. Example DNA showed a direct break in absence of FUS, while at 100 nM FUS, the break was delayed. This delay was accompanied by the fusion of two condensates moving towards each other, visible in the corresponding kymograph and the zoom. Scale bar: 4 µm
(B) Breaks were classified into 'direct' and 'delayed' and the DNA extension at which they occurred was measured. Error functions were fitted to estimate the characteristic extension above which delayed breaks typically occurred. Number of analyzed DNA molecules: 0/1 nM: 96, 10 nM: 29, 100 nM: 29
(C) Illustration of the rupturing process

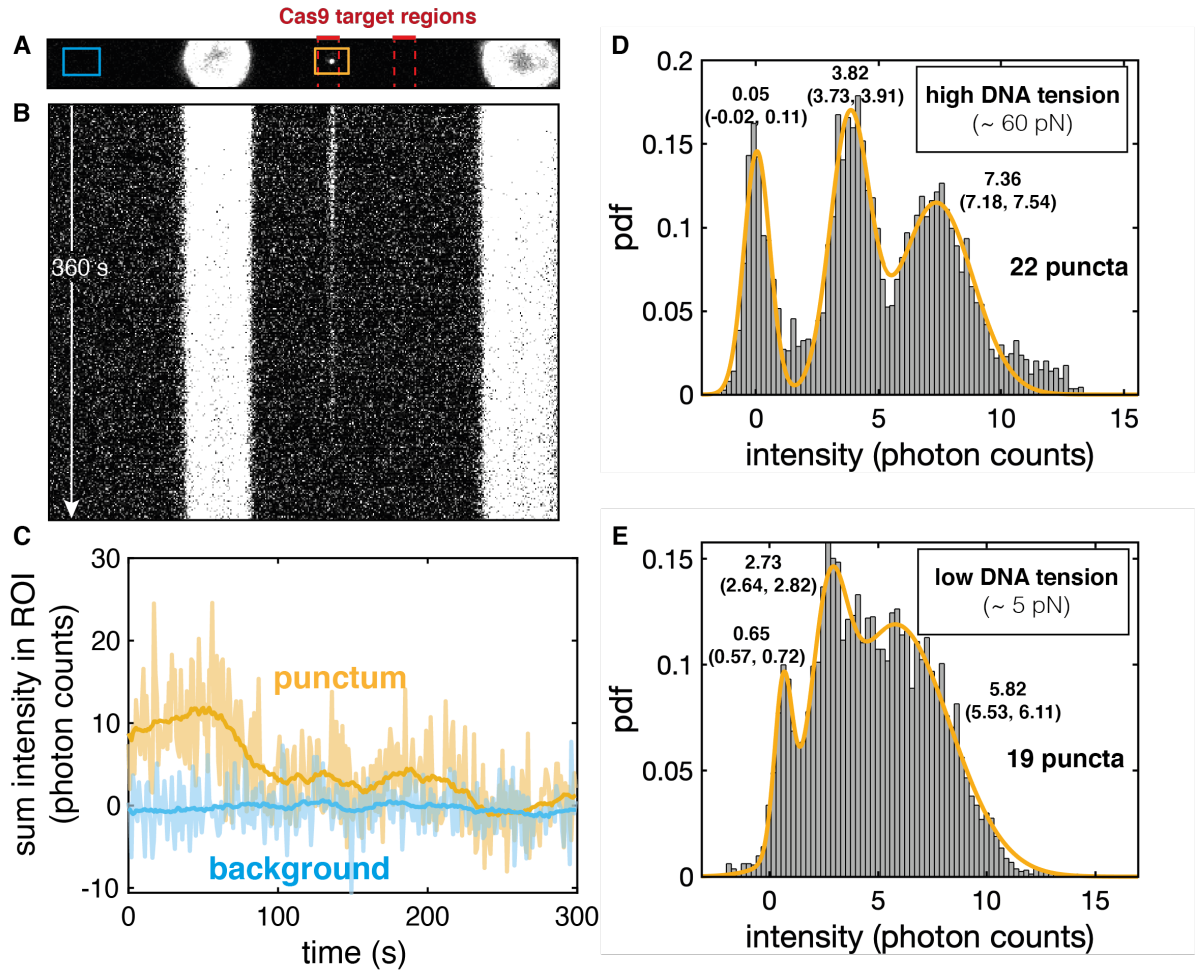

Figure S4. Estimation of single GFP fluorescence intensity using dCas9-GFP

(A) Representative maximum intensity projection image of dCas9-GFP binding to lambda phage DNA. dCas9-GFP was complexed with 4 different guide RNAs corresponding to 4 adjacent sequences localized at ~1/3 of the contour length of lambda phage DNA. dCas9-RNA complexes were incubated with lambda phage DNA before binding of DNA to the beads, resulting in the stable attachment of up to four complexes to the DNA target regions. Imaging was performed with the same settings as the FUS-DNA binding experiments. DNA was held either in an overstretched configuration (18 µm, ~60 pN) or in a relaxed configuration (15 µm, < 5 pN).
(B) Kymograph of the experiment shown in (A), bead size: 4 µm.
(C) Time traces of the summed intensity inside two segments of the imaging ROI (shown in (A). Light blue: background ROI. Orange: ROI containing a punctum that represents multiple dCas9-GFP molecules bound to adjacent sites at ~1/3 of the contour length of lambda phage DNA. The time trace of the punctum shows discrete intensity levels. Over time, intensity decreases, indicative of photo bleaching events. (Transparent lines: raw intensities, bold lines: moving average over 30 frames).
(D) Histogram of intensities (moving average over 30 frames) for imaging experiments performed at high DNA tension. Three Gaussians were fitted to capture the main peaks. They represent the background intensity peak as well as the intensity of one and two GFP molecules. (22 puncta were analyzed).
(E) Histogram of intensities (moving average over 30 frames) for imaging experiments performed at low DNA tension. Three Gaussians were fitted to capture the main peaks. They represent the background intensity peak as well as the intensity of one and two GFP molecules. Peaks are less distinct due to the increased fluctuations of DNA at low tension. Moreover, the intensity found for one GFP is lower (2.73 p.c. compared to 3.82) (19 puncta were analyzed).

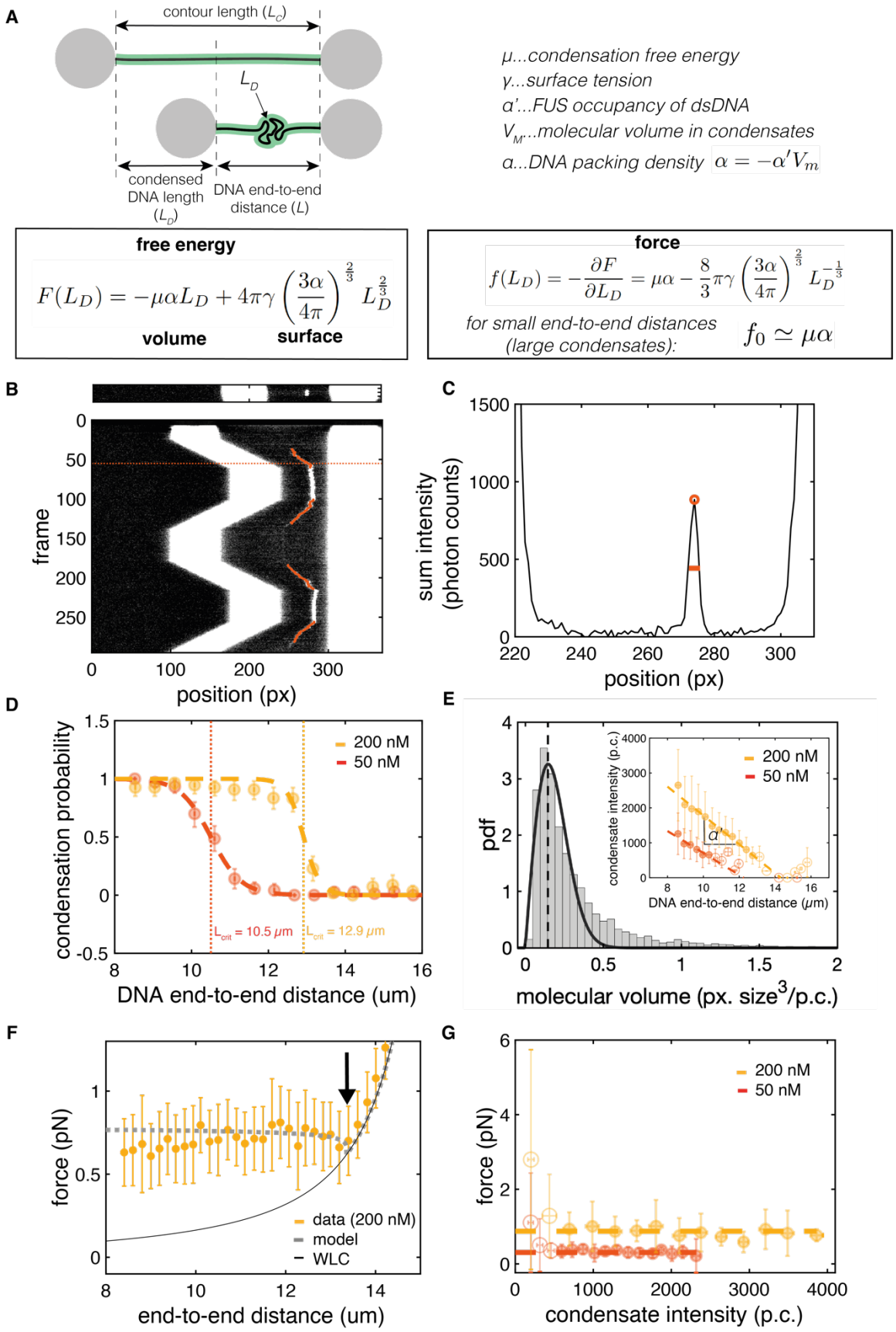

Figure S5. Analysis of FUS-dsDNA co-condensate formation

(A) Model for DNA condensation mediated by protein attachment. The free energy of the condensate containing the DNA length L_D is determined by the volume and the surface tension

of the condensate. α is the packing factor relating the condensed DNA length to the volume of the condensate. The force exerted by the condensate in order to pull in more DNA can be calculated using the negative partial derivative of the free energy with respect to L_D.
(B) Representative snapshot and kymograph of a FUS-dsDNA condensation experiment performed at 200 nM FUS. Overlayed in red: tracked position of the condensate when the trap position is changed. Dashed line marks the snapshot shown on top.
(C) Sum intensity profile of the snapshot shown in (B). Tracked peak and FWHM are marked. For downstream analysis, we approximated the total condensate intensity as the product of peak height and FWHM. FWHM was used as an estimate of the radius of the condensate to calculate its volume (condensate approximated as sphere).
(D) Probability that a condensate forms on a DNA molecule vs. DNA end-to-end distance. FUS-dsDNA condensates form below a critical, FUS concentration dependent DNA end-to-end distance L_{crit}. Circles, binned means; error bars, 95% confidence interval (bootstrapping) ; Red: 50 nM FUS; yellow: 200 nM FUS; dashed lines: error function fits; dotted lines mark concentration dependent L_{crit}.
(E) Estimation of the packing factor α. α is defined as $\alpha = -\alpha' V_m$. α' is the FUS line density on DNA in FUS-dsDNA condensates. Vm is the molecular volume of FUS inside condensates. Large plot: Histogram of the probability density function (pdf) of the ratio of condensate volume and condensate intensity for all tracked condensates. Fit by a Rayleigh distribution function allows to extract the average molecular volume (volume per photon count, V_M) by calculating the expectation value of the function. Data: histogram of 51 condensates that formed on 51 individual DNA molecules, tracked in 4109 frames; black line: Rayleigh function fitted to histogram. Inset: condensate intensity versus DNA end-to-end distance. Same data as in Fig. 6G. Linear functions were fitted to the regions below L_{crit}. Concentration dependent α' is the slope of these functions. Data: red: condensates formed at 50 nM FUS (29 individual DNA molecules); yellow: condensates formed at 200 nM FUS (22 individual DNA molecules). Filled circles: data points classified as 'condensate' (below L_{crit}); open circles: data points classified as 'no condensate' (above L_{crit}). Dashed lines: linear fits indicating the linear increase of condensate size with decreasing DNA end-to-end distance.
(F) Force vs. DNA end-to-end distance curve obtained from minimization of the total free energy (for details see supplementary experimental procedures). Same data as in Fig. 6H. A dip at the transition from WLC to the constant force regime is observed in the experimental data and is captured by a small, but finite surface tension of the condensate of around 0.15 pN/μm (marked by black arrow). Yellow: experimental data at 200 nM FUS, mean ± STD. Dotted grey line: theory curve. Black thin line: Worm-like chain model of naked DNA.
(G) Force vs. condensate intensity plot. Condensates over a broad range of sizes (intensities) coexist at a constant, FUS concentration dependent force. Yellow and red: same data as shown above. Dashed lines: linear fit to the horizontal region, indicating the constant force regime. Only bins with more than one data point are shown.

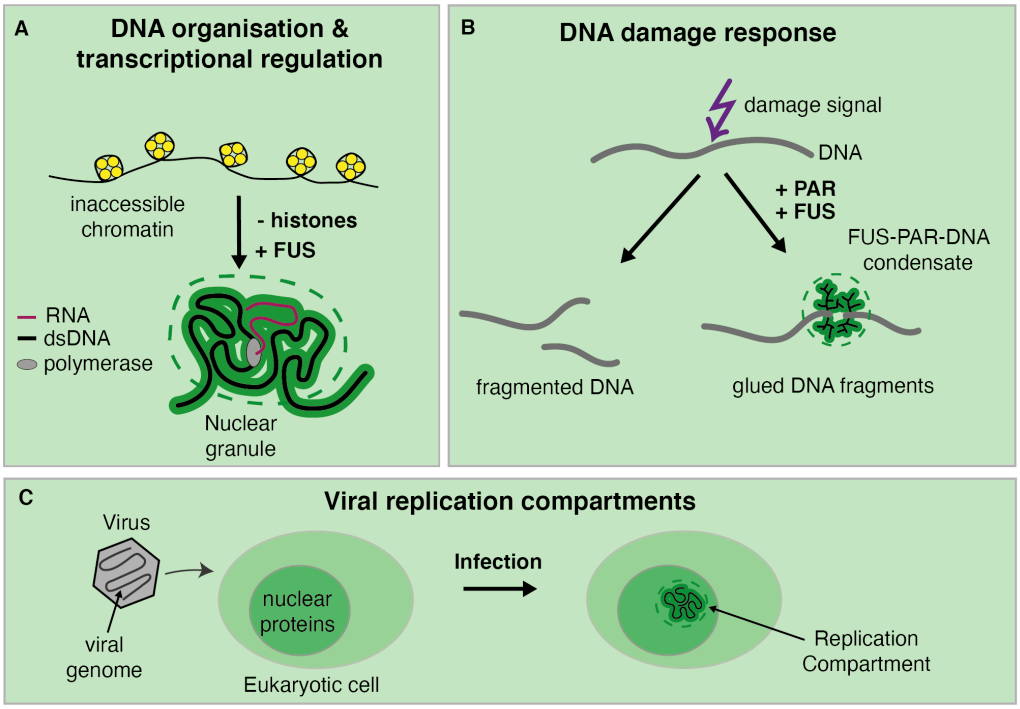

Figure S6. Potential physiological relevance of protein-nucleic acid co-condensation

The mechanism of monolayer protein-nucleic acid co-condensation might be the basis for the formation of (A) dynamic organizational units of highly accessible dsDNA, for example in the context of transcriptional regulation; (B) glue-like inducible DNA damage compartments at PARylated DNA damage sites, or (C) membrane-less Replication Compartments formed by highly accessible viral genomes with hijacked nuclear proteins of infected cells.

Supplementary methods

Analysis of the influence of FUS on DNA rupturing behavior

To study whether FUS influences the rupturing behavior of DNA, individual DNA molecules were transferred into the protein channel. Their extension was continuously increased at 1 μm/s until they broke, starting from 10 μm (Figure S3). Imaging was performed at 1 fps. Breaks observed in the force-extension curves were classified according to the extension at which they occurred and whether they occurred directly (force drop from overstretching plateau to zero within few data points) or in a delayed manner (via multiple intermediate states). The type of breaking event vs. the extension at which it occurred was the plotted for the FUS concentration range between 0 and 100 nM. A characteristic extension for the switch from direct to delayed breaks was estimated using an error function fit. At 100 nM a group of data points indicating direct breaks at around 30 μm extension was excluded from the fit as they probably were associated with rupturing of the DNA at the junctions with the beads rather than being caused by DNA peeling.

dCas9-EGFP preparation, imaging and intensity analysis

Recombinantly expressed dCas9-EGFP was stored at 5.3 mg/ml at -80˚C in storage buffer (250 mM HEPES pH 7.3, 250 mM KCl) and thawed 1 h prior to the experiment. sgRNAs were made using an in vitro expression kit against the following four adjacent target loci on lambda DNA + NGG PAM sequence GGGAGTATCGGCAGCGCCAT TGG, GGAGGATTTACGGGAACCGG CGG, GGCAACCAGCCGGATTGGCG TGG, GGCGGTTATGTCGGTACACC GGG. The spacing between adjacent target sequences was adjusted to 40 to 50 bp to prevent steric hindering of adjacent dCas9-sgRNA complexes. The target region marked by the 4 adjacent RNA sequences corresponds to a region at 1/3 (or 2/3) of the DNA contour. Guide RNAs were expressed and purified using commercial kits (MEGAscript T7 Transcription Kit, Invitrogen and mirVana miRNA isolation Kit, Invitrogen); stored in ddH_2O at 0.6 – 1 mg/mL at -80˚C and thawed together with the dCas9-EGFP protein 1 h prior to the experiment.

First, 2 μL of dCas9-EGFP were pre-diluted into 38 uL complex buffer (20mM Tris-HCl pH 7.5, 200 mM KCl, 5 mM $MgCl_2$, 1 mM DTT) prior to the complexing reaction. Second, 5 μL of the 20x dCas9-EGFP dilution were mixed with 4 μL sgRNA stock which contained all four sgRNAs in equal stoichiometries. Subsequently, the reaction volume was adjusted to 50 μL by adding 41 μL complex buffer and incubated at room temperature (22˚C) for 30 min.

After incubation was completed, the 10 μL of the dCas9-sgRNA complex reaction are mixed with 1 μL of 5 nM biotinylated lambda DNA. The reaction volume was then adjusted to 50 μL by adding 39 μL reaction buffer (40 mM Tris-HCl pH 7.5, 200 mM KCl, 1 mg/mL BSA, 1 mM $MgCl_2$ and 1 mM DTT) followed by a second incubation for 30 min at room temperature (22˚C).

Lambda phage DNA molecules were diluted in FUS buffer and transferred to the microfluidics system of the C-Trap setup. Individual DNA molecules equipped with dCas9-guide RNA complexes were tethered as described before. Fluorescence imaging was performed at 1 fps over 360 frames with a pixel size of 100 nm, a pixel dwell time of 0.05 ms and 5% intensity of the 488 nm excitation laser. DNA molecules were held at a tension of either ~5 pN (‘low tension’) or ~60 pN (‘high tension’).

For image analysis, every frame was background subtracted. Fluorescent puncta sitting at 1/3 or 2/3 of the DNA contour length were segmented and the total intensity within these ROIs was extracted for each frame of each experiment (Figure S4). Note that puncta that were observed outside of the DNA target regions at 1/3 or 2/3 of the DNA contour length were not

considered for analysis as they were suspected to represent dysfunctional and hence potentially aggregated dCas9-EGFP.
For DNA held at low or high tension, the probability density function (pdf) of the intensity inside the ROI in each frame was represented in a histogram. Notably, only up to 3 or 4 clear peaks were visible, indicating that typically not all 4 different dCas-RNA complexes were bound to the target region of the DNA. The peaks were fitted using Gaussian functions and the position of the second peak (the first one depicts the background intensity) was considered to be the approximate intensity of a single EGFP molecule under the corresponding imaging conditions (at high DNA tension: 3.82 ± 0.09 p.c.; at low DNA tension: 2.72 ± 0.09 p.c. (95% confidence interval)).

Towards a full model of the FUS-dsDNA co-condensates held in optical traps

To capture the full force vs. end-to-end distance curve of the FUS-dsDNA condensate in a dual trap optical tweezer experiment, we consider a free energy that contains contributions from the FUS-DNA condensate, the stretched DNA polymer, and the optical traps.
The free energy F_{cond} of the condensate is written as

$$F_{cond} = -\mu\alpha L_D + 4\pi\gamma \left(\frac{3\alpha}{4\pi}\right)^{2/3} {L_D}^{2/3},$$

where μ denotes the condensation free energy per volume, L_D is the length of DNA contained in the condensate, α is the packing factor relating L_D to the condensate volume, and γ is the surface tension (2). The mechanical energy F_{WLC} stored in a stretched DNA polymer is determined by integration of the polymer force f_{WLC} (Worm Like Chain, WLC) (3) according to

$$\boldsymbol{F_{WLC}} = \int_0^{x_D} \boldsymbol{f_{WLC}}(\boldsymbol{x})\, \boldsymbol{dx}\,,$$

with

$$f_{WLC} = \frac{k_B T}{P}\left(\frac{1}{4}\left(1 - \frac{x_D}{L}\right) - \frac{1}{4} + \frac{x_D}{L}\right)^{-2}.$$

Here, T denotes the absolute temperature, k_B is Boltzmann's constant, L is the contour length of the DNA that is not condensed ($L = L_C - L_D$ with L_C denoting the contour length of 16.5 μm of the entire piece of lambda phage DNA), and x_D is the DNA end-to-end distance and thus the separation distance between the surfaces of the two beads in the optical trap. The energy stored in the two optical traps is given by

$$F_{traps} = \frac{K}{4}(S - x_D)^2,$$

where K denotes the stiffness of the optical traps and S is the distance between the two trap centers, minus twice the radius of the beads. Hence, $S - x_D$ denotes the summed displacement of the two beads in the two optical traps. The total free energy of the system F is now given by

$$F = F_{cond} + F_{WLC} + F_{traps}.$$

We consider the ensemble where the distance S between the two trap centers is fixed, and x_D and L_D are fluctuating quantities that approach values that correspond to a minimum of F. We determine this minimum numerically for the following values of the input parameters: $L_C = 16.5$ μm, $k_BT = 4.15$ pNnm, $P = 50$ nm, $\mu = 11.78$ pN/μm^2, $\alpha = 0.059$ μm^2, $\gamma = 0.15$ pN/μm, $K = 0.15$ pN/nm. For a pair of values of L_D and x_D at which F is minimal, we

determine the DNA tension according to $-\frac{\partial F_{traps}}{\partial x_D}$ or partial $\frac{\partial F_{WLC}}{\partial x_D}$. The resulting force vs. end-to-end distance curve was plotted on top of the experimental data obtained for 200 nM FUS (Figure S5F).

Supplementary movies

Movie S1
Continuous overstretching of lambda phage DNA in presence of 100 nM FUS showing homogeneous adhesion of FUS to stretched ssDNA and dsDNA and formation of condensates of FUS with peeled ssDNA (bead size: 4 μm)

Movie S2
Repetitive overstretching of lambda phage DNA in presence of 100 nM FUS, showing reversibility of FUS-ssDNA condensate formation (bead size: 4 μm)

Movie S3
Step-wise overstretching of lambda phage DNA in presence of 100 nM FUS, indicating viscoelastic-like material properties of FUS-ssDNA condensates (bead size: 4 μm)

Movie S4
A single lambda phage DNA molecule attached to a bead and stretched by hydrodynamic flow. Attachment of FUS (100 nM) leads to DNA condensation (bead size: 4 μm)

Movie S5
Repetitive stretch-relax cycles of lambda phage DNA in presence of 100 nM FUS at end-to-end distances below the DNA contour length. Reversible formation of a FUS-dsDNA condensate is observed (bead size: 4 μm)

Movie S6
FUS-mediated reversible zippering of two dsDNA strands studied using three optical traps (bead size: 4 μm)

Supplementary references

1. X. Wang, J. C. Schwartz, T. R. Cech, Nucleic acid-binding specificity of human FUS protein. *Nucleic Acids Research* **43**, 7535–7543 (2015).
2. T. Quail, *et al.*, Force generation by protein–DNA co-condensation. *Nature Physics 2021 17:9* **17**, 1007–1012 (2021).
3. S. B. Smith, Y. Cui, C. Bustamante, Overstretching B-DNA: The elastic response of individual double-stranded and single-stranded DNA molecules. *Science* **271**, 795–799 (1996).